






Single-shot ranging and velocimetry with a CW lidar far beyond the coherence length of the CW laser

MUSTAFA MERT BAYER,^{1,4}  XUN LI,^{1,5}  GEORGE NIKOLAEV
GUENTCHEV,^{1,6}  RASUL TORUN,^{2,7}  JOSE E. VELAZCO,^{3,8} AND
OZDAL BOYRAZ^{1,9} 

¹Electrical Engineering and Computer Science Department, University of California, Irvine, CA 92697, USA

²Informatics and Information Security Research Center (BILGEM), TUBITAK, 41470 Kocaeli, Turkey

³Jet Propulsion Laboratory, Pasadena, CA 91109, USA

⁴bayerm@uci.edu

⁵xunl12@uci.edu

⁶guentchg@uci.edu

⁷rasul.torun@tubitak.gov.tr

⁸jose.e.velazco@jpl.nasa.gov

⁹oboyraz@uci.edu

Abstract: The spectral linewidth of the continuous-wave (CW) lasers is one of the key limitations on the coherent lidar systems, which defines the maximum detection range. Furthermore, precise phase or frequency sweeping requirements are a deterrent in many applications. Here, we present the Phase-Based Multi-Tone Continuous Wave (PB-MTCW) lidar measurement technique that eliminates the necessity of using high coherence laser sources as well as any form of phase or frequency sweeping while employing coherent detection. In particular, we modulate a CW laser source with multiple radio-frequency (RF) tones to generate optical sidebands. Then, we utilize the relative phase variations between the sidebands that are free from laser phase noise to calculate the target distance via post-processing and triangulation algorithms. We prove that the PB-MTCW technique is capable of performing single-shot ranging and velocimetry measurements at more than 500× the coherence length of a CW laser in a benchtop experimental demonstration. Overall, precise phase or frequency sweeping requirements and the spectral linewidth of CW lasers, which defines the maximum detection range, are the key limitations of long-distance coherent lidar systems. The proposed approach overcomes these limitations and enables single-shot ranging and velocimetry measurements, especially for long-range applications such as spacecraft and airborne coherent lidars.

© 2021 Optical Society of America under the terms of the [OSA Open Access Publishing Agreement](#)

1. Introduction

Digital cameras, radars, and lidars (light detection and ranging) are considered to be three enabling technologies in autonomous terrestrial and aerial vehicles [1,2]. Lidars, the optical version of radars, operate by generating a point cloud of the environment based on the information encoded in the echoed light. The emerging needs of high resolution ranging and imaging in the areas such as terrestrial altimetry fueled the interest in lidar systems [3,4]. Lidars perform ranging by either measuring the time-of-flight (ToF) of a laser pulse traveling from laser source to a target and back to a photodetector, or by generating the so-called radio frequency (RF) beat tones through the interference of reference light and the reflected light from a target by using continuous wave (CW) laser and a coherent detection system [5–11]. The conventional ToF lidars provide a robust ranging methodology by using high peak power laser impulses. However,

velocity information of a target-in-motion can only be mined through a comparison of consecutive frames, which is in practice prone to errors due to interference and the movement of the target [12,13].

Alternative lidars utilizing coherent detection have the capability to perform simultaneous ranging and velocimetry by exploiting the Doppler effect [14–16]. Nowadays, coherent detection is utilized by amplitude-modulated continuous-wave (AMCW) [17] and frequency-modulated continuous-wave (FMCW) lidars [6–9]. In these approaches, a linearly chirped, frequency-swept, or phase-swept laser beam is transmitted to the target. The back-reflected signal interferes with a fraction of the swept laser source that acts as the reference beam and generates a radio frequency beating tone at the photodetector. The phase or the frequency of the beating tone is used to extract the range information. In the case of FMCW lidar, for instance, the range is measured based on the frequency of the tone, which corresponds to the difference between the instantaneous frequencies of the reference and the collected signal at the time of the interference measurement [18–21]. The encoded Doppler shifts in the resultant frequencies provide the velocity information simultaneously. However, the maximum measurable distance in coherent lidars is not solely limited by the power of the source, but by the quality of the laser [22,23]. In other words, the optical linewidth (Δf) of the CW laser in a coherent lidar dictates the coherence length of the light as $L_{coh} = c/\pi\Delta f$, where c is the vacuum velocity of light [24]. The lidar operation beyond the coherence length of the laser can result in degradation of the signal quality due to the random laser phase noise and yields an error in the measurements [23,25]. The narrow-linewidth lasers, which have lower phase noises, are the solution for the coherence, but the cost of such lasers is a concern for the commercialization of coherent lidars. Similarly, fast and linear frequency sweeping requirements along with potential laser stability issues exhibit another challenge in terms of electronics for such lidars along with the temporal coherence of the laser [6].

Interferometric detection and ranging methods and random amplitude modulation techniques were investigated previously to compensate for the impact of laser phase noise with dual-frequency heterodyning systems [26–29]. In these methods, either two subsequent measurements with slightly different modulation frequencies were performed to compensate for the unambiguous range [26] or multiple wavelengths were used to compute the target range. Transferring these techniques to FMCW lidars alleviates phase noise but frequency sweeping remains a challenge for long-range applications [31].

Previously, Multi-Tone Continuous Wave (MTCW) lidar relying on the phase and amplitude variations has been studied for single-shot ranging and velocimetry [30–37]. In those experiments, we have used amplitude variations due to constructive or destructive interferences at selected RF tones generated by free-running RF sources for ranging. Similarly, instead of amplitude variations, we have also utilized the phase variations in the RF tones to perform ranging [32,37]. The experimental setup and relevant algorithms in phase measurements use a fraction of the modulated source laser as a reference to facilitate extraction of absolute phases of individual RF tones, which includes the phase variations in the reference and the phase of the echo signal, to extract valuable ranging information. Such an approach, similar to FMCW lidar suffers from coherence length limitations.

Here, we hypothesize that if we use a fraction of the source laser before encoding the RF tones at the amplitude modulator, and use proper algorithms in a new experimental setup, we can come up with a solution that removes the common noise terms and impact of coherence length limitations. In this technique, which we call it Phase-Based Multi-Tone Continuous Wave lidar (PB-MTCW), instead of employing any form of frequency, phase, or amplitude sweeping, we modulate a CW laser with multiple phase-locked radio-frequency (RF) tones to generate stable sidebands using a Mach-Zehnder modulator (MZM) under a linear modulation configuration. Then we utilize the phases of individual tones that are encoded in the echo signal after heterodyning with the unmodulated local oscillator as demonstrated in Fig. 1(c). Since the absolute value of the phase

differences between the reference, i.e. local oscillator, and the echo signal are impaired due beyond the coherence length of the laser, we utilize the phase differences between RF tones that are free from common noise terms. The phase difference of the individual sidebands reveals the target distance, while the acquired Doppler shift produces the target velocity, simultaneously. Here, we present theoretical and experimental proof of single-shot ranging and velocimetry measurements at more than $500\times$ (limited by the experimental setup) the coherence length of the

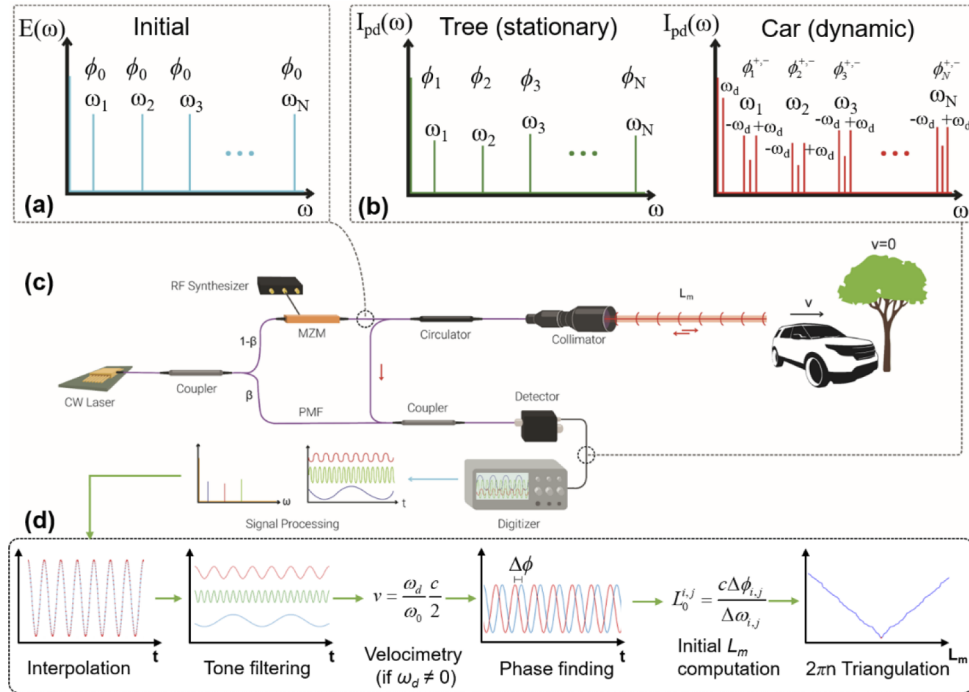


Fig. 1. Working principle of the Phase-Based Multi-Tone Continuous Wave Lidar. (a) The electric field spectrum of the laser after modulation with $\omega_1, \omega_2, \omega_3, \dots, \omega_N$ frequencies by a Mach-Zehnder modulator (MZM) before leaving the collimator. Each tone has an initial phase of ϕ_0 before ranging. (b) The resultant photocurrent (I_{pd}) spectra after acquiring the echoed signal from a stationary tree and a car in-motion with a velocity (v), respectively. The tones accumulate different phases of $\phi_1, \phi_2, \phi_3, \dots, \phi_N$ with respect to the target distance L_m . In the case of the dynamic target, the optical carrier and the sidebands realize a Doppler frequency shift of ω_d . ϕ_i^{+-} represents the acquired phases of each Doppler-shifted modulation. (c) Schematic design of the proposed PB-MTCW lidar. A continuous-wave laser is split into two through a fused fiber coupler with a coupling coefficient of β . All the fibers are polarization-maintaining (PMF) to inhibit potential polarization mismatches. The measurement branch of the system is further modulated by an MZM with multiple RF tones generated by phase-locked RF synthesizers operating with a common clock. The modulated light is then fed to a circulator that is followed by a collimator for both transmission and reception. The collected light is sent to a second coupler for heterodyning with the local oscillator branch, which is further connected to a high-speed photodetector. (d) The flowchart of the signal processing starts with the interpolation of the time-domain data. Each modulation tone or shifted peak is filtered out for post-processing. If $\omega_d \neq 0$, the target speed is computed, then the individual tone phases are generated. Using the phase difference between the tones, the initial target distance ($L_0^{i,j}$) is computed, which is followed by the triangulation of the actual target distance with multiple $L_0^{i,j}$ to achieve ranging.

laser. Experimental results show that there is a negligible difference in measurements performed by a highly coherent laser and low coherence laser. Hence, the novel experimental system and signal processing algorithms presented here pave the way for lidar measurements beyond the existing capabilities of the current phase-based lidar technologies.

2. Concept of phase-based multi-tone continuous wave lidar

To give a brief theory of the proposed concept let's assume that an amplitude-modulated CW laser source emits a light toward the target with an electric field profile as shown in Eq. (1) and the corresponding spectrum is illustrated in Fig. 1(a).

$$E_{out} = \frac{A_0}{\sqrt{2}} \alpha_f \sqrt{1 - \beta} \left(\exp(j\omega_0 t + j\phi_0 + j\phi_n(t)) - \frac{m}{4} \sum_{i=1}^N \left(\exp[j(\omega_0 + \omega_i)t + j(\phi_0 + \phi_i^{RF}) + j\phi_n(t)] + \exp[j(\omega_0 - \omega_i)t + j(\phi_0 - \phi_i^{RF}) - j\phi_n(t)] \right) \right) \quad (1)$$

The ω_0 and ω_i indicate the angular frequency of carrier and i^{th} tone among a total of N tones, respectively, and ϕ_i^{RF} is the initial phase of the corresponding RF modulation, which is locked to a fixed value for all tones. A_0 is the field amplitude of light, m represents the modulation depth, β is the coupling coefficient of the fiber coupler, α_f depicts the fiber loss. The reflected signal from a target that is L_m meters away will be Doppler shifted if the target is nonstationary. The current generated at the photodetector after the interference of the echoed signal and the reference signal (unmodulated source laser) can be expressed without the DC contribution (I_{DC}) as in Eq. (2).

$$\begin{aligned} I_{pd} = I_{DC} &+ \frac{\alpha_m}{\sqrt{2}} A_c \cos \left(\omega_d t + \frac{2L_m}{c} \omega_0 + \frac{L_m}{c} \omega_d + \Phi(t, \tau) \right) \\ &- \frac{\alpha_m^2}{8} A_s \sum_{i=1}^N \cos \left(\omega_i t + \frac{2L_m}{c} \omega_i + \phi_i^{RF} \right) + \frac{\alpha_m^2}{16} A_s \sum_{i=1}^N \cos \left(2\omega_i t + \frac{4L_m}{c} \omega_i \right) \\ &- \frac{\alpha_m}{2\sqrt{2}} A_c \sum_{i=1}^N \cos \left((\omega_i + \omega_d)t + \frac{2L_m}{c} (\omega_0 + \omega_i) + \frac{L_m}{c} \omega_d + \phi_i^{RF} + \Phi(t, \tau) \right) \\ &- \frac{\alpha_m}{2\sqrt{2}} A_c \sum_{i=1}^N \cos \left((\omega_i - \omega_d)t - \frac{2L_m}{c} (\omega_0 - \omega_i) - \frac{L_m}{c} \omega_d - \phi_i^{RF} - \Phi(t, \tau) \right) \end{aligned} \quad (2)$$

The optical carrier will experience a Doppler frequency shift (ω_d) that is proportional to the velocity of the target (v) by $\omega_d = (2v/c)\omega_0$ [15] as indicated in Fig. 1(b). Here, $A_c = Rm\sqrt{\beta}\sqrt{1 - \beta}A_0^2\alpha_f^2$ is the amplitude of the cross-beating terms and $A_s = Rm(1 - \beta)A_0^2\alpha_f^2$ is the amplitude of the self-beating terms, where R is the responsivity of the detector and α_m represents the scattering loss. The phase noise of the CW laser before and after a travel time $\tau = 2L_m/c$ are $\phi_n(t)$ and $\phi_n(t - \tau)$. Therefore the phase difference due to laser phase noise can be represented as $\Phi(t, \tau) = \phi_n(t) - \phi_n(t - \tau)$ [38]. If the target is static, the resultant I_{pd} equation will be

$$\begin{aligned} I_{pd} = I_{DC} &- \frac{\alpha_m}{2\sqrt{2}} A_c \left[\sum_{i=1}^N \cos \left(\omega_i t + (\omega_0 + \omega_i) \frac{2L_m}{c} + \phi_i^{RF} + \Phi(t, \tau) \right) + \sum_{i=1}^N \cos \left(\omega_i t - (\omega_0 - \omega_i) \frac{2L_m}{c} - \phi_i^{RF} - \Phi(t, \tau) \right) \right] \\ &+ \frac{\alpha_m^2}{8} A_s \left[\sum_{i=1}^N \cos \left(\omega_i t + \omega_i \frac{2L_m}{c} + \phi_i^{RF} \right) + \sum_{i=1}^N \cos \left(\omega_i t + \omega_i \frac{2L_m}{c} - \phi_i^{RF} \right) \right] + m \frac{\alpha_m^2}{8} A_s \sum_{i=1}^N \cos \left(2\omega_i t + \omega_i \frac{4L_m}{c} \right) \end{aligned} \quad (3)$$

Our goal is to develop an algorithm that can calculate the phase and frequency information independent of common noise terms, and then extract the velocity and range of the target. In the case of dynamic targets, $A_i \cos \left((\omega_i \pm \omega_d)t \pm \frac{2L_m}{c} (\omega \pm \omega_i) \pm \frac{L_m}{c} \omega_d \pm \phi_i^{RF} \pm \Phi(t, \tau) \right)$ can be used to define a single tone. As is clearly seen from this definition, a frequency shift in the carrier

frequency or any tone frequencies reveals the Doppler shift, and hence the velocity of the target [31,32]. However, range information is stored in the phase term and it is mixed with noise terms. To eliminate the common noise terms we mix two of these individual tones at ω_i and ω_j ($i \neq j$), either electronically or in the digital domain, the resultant intermediate frequency (IF) tone will be $A_i A_j \cos(\Delta\omega_{i,j}t \pm \Delta\phi_{i,j})$, where $\Delta\phi_{i,j}$, and $\Delta\omega_{i,j}$ are the phase and frequency differences of i^{th} and j^{th} tones, respectively. For proof of concept, we performed digital signal mixing to acquire the phase of the IF tones after digitally filtering the static modulation frequencies via narrow bandpass filters. As a result, the common phase and frequency terms related to the optical carrier and the Doppler shift are eliminated with inter-tonal mixing that also eliminates the impact of the coherence length of the laser. Similarly, we can use RF mixing of carrier frequencies of a static target with individual tones defined as $2A_i \cos\left(\frac{2L_m}{c}\omega_0 + \phi_i^{RF} + \Phi(t, \tau)\right) \cos(\omega_i t + \frac{2L_m}{c}\omega_i)$, to eliminate common noise terms. After the RF mixing, the phase of IF tones will be free from phase and the amplitude noise of the source and reveal only the range information of the target: $L_m = (2\pi n + \Delta\phi_{i,j})c/\Delta\omega_{i,j}$, where n is an integer. As a result, PB-MTCW lidar methodology is immune to the phase variations induced by the laser phase noise, and hence it is possible to perform ranging beyond the coherence length of the laser.

The modulo- 2π cyclic behavior of phase will lead to a periodic range estimation. Similar to global positioning systems that use multiple satellites to triangulate the exact position, we need redundancy of multiple agents for accurate range information. Here, we use multiple RF tones to pinpoint the value of L_m by using a triangulation algorithm. In particular, for a given $\Delta\phi_{i,j}$, which corresponds to $\Delta\omega_{i,j}$ the total length will be $L_m = nL^{i,j} + L_0^{i,j}$, where the spatial period is $L^{i,j} = 2\pi c/\Delta\omega_{i,j}$ and the residual length is $L_0^{i,j} = c\Delta\phi_{i,j}/\Delta\omega_{i,j}$ [35]. If the integer value of n is swept, the potential L_m values can be computed for each $\Delta\omega_{i,j}$. After concatenating all the possible combinations of L_m into a data matrix $M_{k,l}$, where k is equal to the predefined sweep limit (n_{max}) that is set according to the maximum expected range, and l is the number of available $\Delta\omega_{i,j}$

combinations. The standard deviation of each row is calculated as $\sigma_k = \sqrt{\sum_{r=1}^l (M_{k,r} - \bar{M}_k)^2 / l}$

[35], where \bar{M}_k , the mean of the k^{th} row, which yields the minimum σ_k corresponds to the actual target distance L_m as depicted in Fig. 1(d). However, the minimum σ repeats itself at every $L_{rep} = 2\pi c/\omega_{gcd}$, where ω_{gcd} stands for the greatest common divisor of the $\Delta\omega_{i,j}$, such phenomenon is called an unambiguity length in lidar systems [35]. One way of avoiding recursive solution or unambiguity length is the selection of the tones in a fashion to make sure L_{rep} is longer than the maximum expected range. For extremely long measurement lengths, instead of using very low-frequency modulation tones to increase L_{rep} , an introduction of a quasi-CW pulsation will be more advantageous. Not only that such a quasi-CW approach facilitates time gating to generate coarse range information without unambiguity length limitation, but also results in higher signal-to-noise ratio measurements compared to an equal power pure CW approach. This approach along with the post-processing in the PB-MTCW approach is illustrated as a block diagram in Fig. 2. The complete theoretical model and details about triangulation are in Supplement 1.

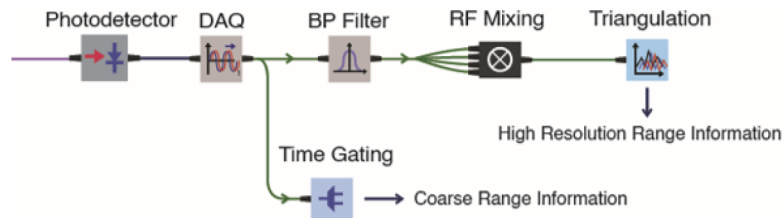


Fig. 2. Block diagram representing the post-processing after data acquisition. The I_{pd} is first captured by a data acquisition board (DAQ). The coarse range information through quasi-CW pulses is computed via time gating. The data is processed by filtering out individual tones via bandpass (BP) filters. Each tone is RF mixed to yield the intermediate frequencies (IF). The phase and frequency of the final IF tones are used in the triangulation algorithm to generate the high-resolution range information.

3. Methodology

The testbench in Fig. 3 is built by using two different lasers. The highly coherent 1064nm laser diode has <100kHz linewidth (RPMC Lasers - R1064SB0300PA) and the output optical power is set to ~50mW. The low coherence 1064nm laser has a 5.3GHz linewidth (QPhotonics - QFBGLD-1060-100) and operates at the same output levels. The characterization details of the low coherence laser are in Supplement 1. All the fibers in the optical system are polarization-maintaining (PMF 980) to prevent polarization mismatching to achieve beating. The CW laser is followed by an isolator and then split into two branches. The local oscillator arm is pigtailed to a collimator. The measurement branch is connected to a high-speed Mach-Zehnder electro-optic modulator (iXblue – NIR-MX-LN series), which is optimized for 1064nm and has a 30dB extinction ratio. The MZM is biased near the quadrature point that is 1.6V. The modulation tones are set through phase-locked RF synthesizers (Windfreak Technologies - SynthHD (v2)) and their phase matching is realized through a trigger clock of 10MHz provided by a stable frequency generator. The same clock triggered the oscilloscope (Tektronix - MDO34) with 1GHz bandwidth to achieve robust phase measurements. The oscilloscope is set to have a 200 μ s time window with a 5GSa/s sampling rate (10^6 data points). Phase-locked RF frequencies are transmitted to MZM after getting combined in a 4-way RF power splitter (Mini Circuit - ZN4PD1-63HP-S+). The modulated light inside the PMF is brought to free space through an additional collimator. The two collimators are placed in a fashion to form a cross-like configuration. A 1064nm 50/50 beamsplitter is placed at the intersection point of two light beams. Light coupling to the free space high-speed PIN photodetector (Thorlabs – DET08C) is optimized with a microscope lens. The stage carrying the target reflector is placed and aligned ~83cm away from the output facet of the BS. A free-space optical attenuator with a total of ~20dB attenuation is placed on the path of propagation to mimic the potential scattering losses.

Moreover, tone selection plays a vital role in PB-MTCW lidar. Here, we have a full frequency range from 0Hz to multi GHz (limited by the detection system) and we don't have dictated carrier frequencies. The tones are selected in a fashion to prevent any second and third harmonic overlaps to maximize the spur-free dynamic range (SFDR). Operating close to the linear modulation regime of the MZM reduces the strength of the harmonics, as well. Each RF tone is set to have an amplitude of 90mV_{pp}, hence the corresponding m is 0.07 per tone indicating a close-to-linear operation. Similarly, intermodulation tones are selected to forestall possible frequency matchings to preserve the purity of tone phases and to improve crosstalk and SFDR. Even though a low modulation index is utilized in the experiment, this is not a hard limit for the PB-MTCW operation. Further optimization on the modulation index can be performed by considering the potential SFDR and signal-to-noise ratio (SNR) requirements. The tones are selected in a fashion

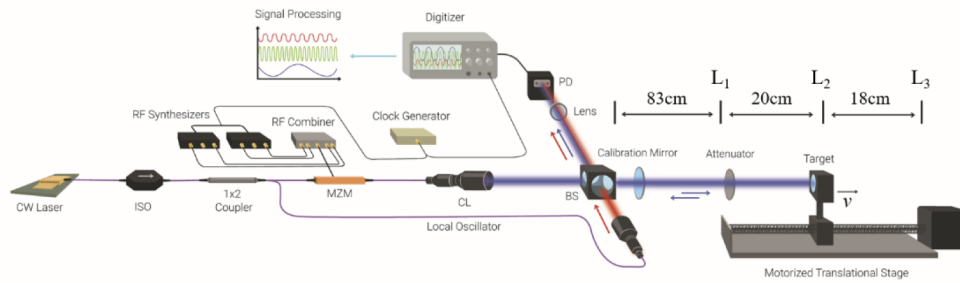


Fig. 3. Schematic representation of the experimental test bench. First, a 1064nm CW laser with $<100\text{kHz}$ linewidth ($L_{\text{coh}} \sim 1\text{km}$), then another 1064nm CW laser with 5.3GHz linewidth ($L_{\text{coh}} \sim 18\text{mm}$) is used to demonstrate ranging further than the laser coherence length. The source is followed by a fiber isolator (ISO), which is connected to a 1x2 fiber coupler to realize the unmodulated local oscillator. The measurement branch is modulated through an MZM with 3RF tones via phase-locked RF synthesizers that are triggered by a clock generator, which also triggers the digitizer. The outputs of both branches are connected to two separate collimators (CL). A free-space optical beamsplitter (BS) is placed in front of both CLs to realize beating after collection on the photodetector (PD). The motorized stage carrying the target reflector is anchored 83cm away from the output facet of the BS. Three measurement distances are $L_1 \sim 83\text{cm}$, $L_2 \sim 103\text{cm}$, and $L_3 \sim 121\text{cm}$ for stationary target ranging. v represents the target speed during dynamic target ranging.

to prevent any second harmonic overlaps. Similarly, intermodulation tones are calculated to forestall possible frequency matchings to preserve the tone phases. Moreover, the tones should be phase-locked, and to achieve this, the tones that are divisible by the trigger frequency of 10MHz are selected. In this experiment, tones are selected as 500, 700, and 950MHz, which satisfy the aforementioned conditions. The greatest common divisor of these tones is 50MHz that indicates the unambiguity length of the resultant minimum standard deviation point is $\sim 3\text{m}$ to generate the target distance. Since the target is set to $<3\text{m}$, the unambiguity length didn't alter the results. The impact of the number of modulation tones is presented in [Supplement 1](#) via simulation results.

After setting the system parameters, PB-MTCW lidar is calibrated before performing the measurements by placing a dummy mirror 6.5cm away from the BS. This calibration allows the system to acquire the initial tone phases due to the initial phase of the RF synthesizers and the fiber path length. The post-processing algorithm generates a pseudo measurement distance at the position of the dummy mirror based on the measured tone phases after averaging results of 10 trials. This pseudo calibration range is set as the zero-point for the lidar and the ranging measurements are adjusted accordingly by considering the excess 6.5cm, as well.

Data acquisition is further followed by digital signal processing. The measurement data generated by the oscilloscope is interpolated to 2^{23} data points to improve the resolution that eliminates potential distortions during phase calculations since the phases are highly dependent on the time resolution. The time-domain data is converted to frequency domain through fast Fourier transform to localize the modulation frequencies and get the Doppler frequency if the target is in motion. The algorithm scans the interval between the first tone and the baseband to obtain the Doppler shift. The signal is then further processed by a digital second-order bandpass Butterworth filter with a 1MHz bandwidth around each measured modulation tone. The phase of the filter is compensated by performing zero phase distortion filtering that is processing the input data in both the forward and reverse directions [39]. Reduction of the filter bandwidth per individual tone can further enhance the signal-to-noise ratio of the acquired RF signal based on the relationship between noise and electronic bandwidth. The refined tones are then compared with frequency-matched 0-phase digital cosine signals, which yield the phase of the individual

tones. Then the triangulation is performed by setting the sweep length of the integer n to 20, which allows the system to span up to $\sim 15\text{m}$.

4. Experimental verification

To prove the proposed concept two separate sets of experimental measurements on dynamic and static targets are performed. In particular, we conducted ranging and velocimetry measurements on the dynamic target and only the ranging measurements on the static target. Both experiments are performed by using a highly coherent laser with 100kHz linewidth and about 1km corresponding coherence length, and a low coherence laser with 5.3GHz linewidth and about 1.8cm corresponding coherence length. In both cases, we use a reflector as a target that is placed on a motorized translational stage with a maximum speed of 11cm/s in motion. In each experiment, the effective optical path difference between the reference signal and the measurement arm is about 9m, where about 2m of this path difference is in free space and the rest is in fiber. While this path difference is about $100\times$ smaller than the coherence length of the first laser, it is about $500\times$ larger than the coherence length of the second laser. In existing CW lidars, the second laser should not work at such path difference. 10 consecutive measurements are performed to verify results for each set.

In the case of the dynamic target, FFT is performed after data acquisition and the resultant RF spectra were scanned with the algorithm to acquire the Doppler frequencies and the instantaneous target speed as demonstrated in Fig. 4(a) and Fig. 4(b) for high and low coherence lasers, respectively. In the case of the low coherence source, we observe the RF spikes placed on broadband background due to the linewidth of the laser that is measured to be $\sim 5.3\text{GHz}$. Phase measurements are performed by using narrowband RF filtering of these RF spikes. The measured instantaneous velocity for each trial along with the current position information is tabulated in Table 1. The measured Doppler shifts vary between 177.5kHz – 212.5kHz that yields a target speed between 9.44cm/s – 11.3cm/s when the high coherence laser is employed. Similarly, with the low coherence source, the measured velocities are in the range of 9.18cm/s -11.3 cm/s. Therefore, we observe that the measured velocities with high and low coherence lasers are in close agreement that matches the specifications of the motor operating on the stage. The difference is attributed to the fact that the electrical motor accelerates and decelerates very rapidly due to the limited stage length, thus the reflector speed varies. The velocimetry resolution is associated with the frequency resolution ($d\omega$) of the RF spectrum, which can be formalized as $\Delta v = (\pm d\omega/\omega_0)c$. In this experiment, the achieved velocity resolution is $\sim 0.53\text{cm/s}$ due to the 5kHz frequency resolution. In addition, it is possible to resolve the direction of the motion either by using a single-sideband (SSB) modulation instead of a standard dual-sideband modulation [34], where the direction of the Doppler-shifted modulation tones will yield the motion vector or by comparing the multiple frames of the same dynamic target in the software domain.

The range triangulations of the moving target by using high and low coherence lasers are illustrated in Fig. 4(c) and Fig. 4(d), respectively. The measurements are performed while the target is moving around a distance that is about 1m away from the beamsplitter, which is also indicated as L_2 (1.03m) in Fig. 3. Data are captured by using a manual trigger, and hence there is a slight variation in the actual range of the target at each measurement. Among 10 trials with a high coherence laser, range measurements vary between 0.92m and 1.02m. Similar measurements with a low coherence laser yield a range measurement that changes between 0.97m to 1.08m. The ranging resolution is proportional to the time resolution of the system that is computed as $\sim 1\text{cm}$ after interpolation. On the other hand, along with the global minimum, several local minima points appear in the calculation. The response of the triangulation algorithm will be improved by increasing the number of phase-locked RF modulation frequencies, and hence these local minima will disappear.

In the case of stationary target ranging, the reflector is placed at three different locations as $L_1 \sim 83\text{cm}$, $L_2 \sim 103\text{cm}$, and $L_3 \sim 121\text{cm}$ as illustrated in Fig. 3. As a sanity check, the coarse

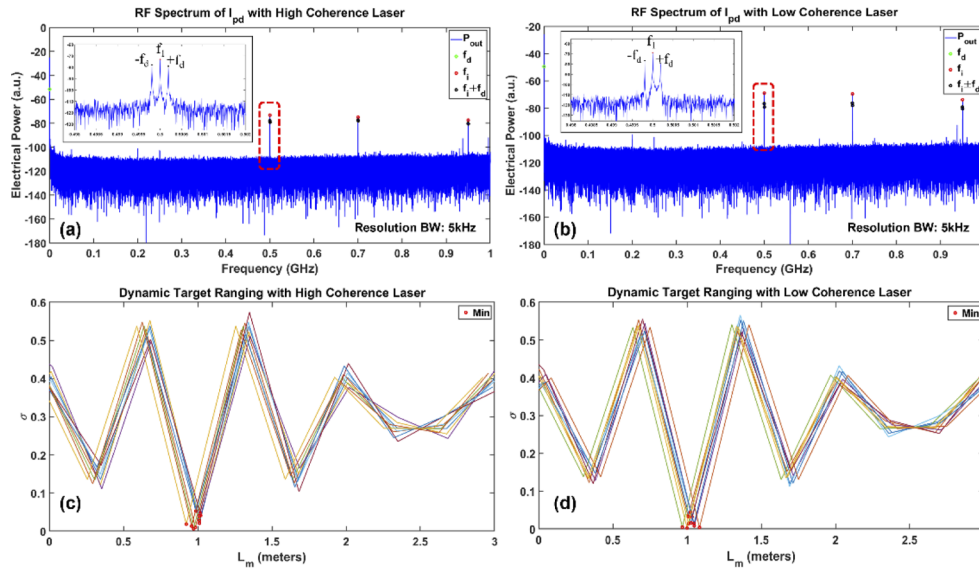


Fig. 4. Dynamic target ranging results with high and low coherence lasers. (a) Acquired I_{pd} spectrum using the $<100\text{kHz}$ linewidth laser of one measurement with a dynamic target, where the tones and the Doppler-shifted frequencies are indicated. The inset magnifies the vicinity of 500MHz tone displaying the $f_1 \pm f_d$ peaks. (b) Similar I_{pd} spectrum using the 5.3GHz linewidth laser. (d) Results of the triangulation algorithm using the highly coherent laser that represents the ranging of the moving target for 10 trials, where the L_m corresponding to the minimum σ yields the target distance. (e) Ranging results using the low coherence laser.

Table 1. Simultaneous ranging and velocimetry results of the dynamic target with both lasers.

High Coherence Laser		Low Coherence Laser	
Range (cm)	Velocity (cm/s)	Range (cm)	Velocity (cm/s)
101.18	10.51	102.68	10.51
98.44	10.51	100.74	10.24
101.18	9.98	101.01	9.98
102.01	9.44	104.91	10.51
97.29	9.98	96.84	9.98
100.93	10.24	102.52	10.24
101.61	11.31	103.40	9.18
98.83	9.98	104.7	11.31
95.97	10.24	108.45	10.24
92.33	10.51	100.07	9.71

measurements of the target distances from the output facet of the BS are performed by using a measuring tape with an estimated precision of $\pm 1\text{cm}$. The ranging measurements while the target is placed at L_2 with a high coherence laser source are presented in Fig. 5(a). The mean value of the measured target distance for L_1 , L_2 , and L_3 are 83.13cm, 102.64cm, and 120.44cm, respectively. Hence, the displacements between L_1 - L_2 and L_2 - L_3 are measured as 19.51cm and 17.81cm. Moreover, the ranging resolution, ΔL , achievable by an individual tone is defined by the minimum distinguishable phase of the i^{th} tone, $d\phi_i$, as $\Delta L \sim \frac{d\phi_i}{\omega_i} c$. Here, $d\phi_i$ depends on various

parameters such as sampling rate, jitter, total noises in the system, surface roughness under the spot size, etc. Nonetheless, it is possible to formalize the minimum theoretical resolution by considering a noise-free case, where $d\phi_i = \omega_i \times dt$, and hence $\Delta L = c \times dt$, where dt is the time resolution. After digitally interpolating the data, the final dt becomes ~ 24 ps, while it was 200ps before interpolation. Based on $\Delta L = c \times dt$, the theoretical minimum resolution is calculated as 0.72cm. The resultant standard deviations for each set of data are < 1 cm, which verifies the ranging precision of the PB-MTCW methodology. The small changes during the stationary target ranging measurements can be attributed to the sampling jitter and noise in the system that distorts the $d\phi_i$.

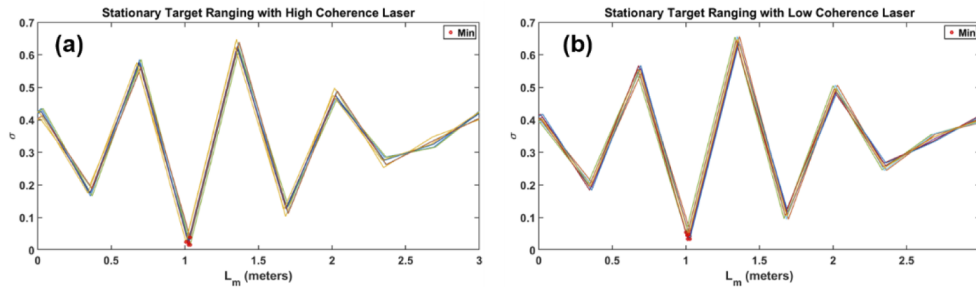


Fig. 5. Stationary target ranging results with high and low coherence lasers via the PB-MTCW technique. (a) Stationary target ranging results of 10 trials while the target is placed at L_2 (~ 1.03 m) using the narrow linewidth laser. (b) Stationary target ranging results at the same position using the low coherence light source.

The same set of measurements are performed for the similar three positions using the low coherence laser and the results for L_2 are presented in Fig. 5(b). Here, the mean values of the trials per location are 82.29cm, 101.79cm, and 121.24cm, respectively. Similarly, the standard deviation of the acquired data is < 1 cm for all positions. As a result, this proves that the PB-MTCW lidar is capable of ranging a target placed at $> 500\times$ larger than the coherence length of the CW laser. It is important to note that $500\times$ is limited by the current measurement setup. The extended experimental results are given in Supplement 1.

5. Discussion and conclusion

Overall, we introduced the Phase-Based Multi-Tone Continuous Wave lidar that enables simultaneous ranging and velocimetry beyond the coherence length of the CW laser. This new approach has the potential to overcome maximum-range limitations for coherent systems, particularly for long-range applications such as satellite-based systems or surface mapping with airborne lidars for oceanography and forestry. Here, we described the working principle of PB-MTCW lidar and the corresponding post-processing approach to extract the valuable ranging and velocimetry information. We presented the stationary target ranging results using a high coherence laser with less than 100kHz linewidth and a low coherence laser with 5.3GHz linewidth, which corresponds to coherence lengths of more than 1km and about 1.8cm, respectively. The measurement variations were found to be < 1 cm for both experiments. Finally, the dynamic target velocimetry and ranging are demonstrated with a target moving at a maximum speed of 11cm/s. It is observed that the same methodology is applicable for moving targets even with a low coherence laser.

A potential implementation of the proposed PB-MTCW lidar to long-range measurements, such as airborne lidar or satellite-based measurements, can utilize so-called quasi-CW lasers (pulsed laser with very broad pulse width). Since the peak power of pulses will be much larger than its multi-tone modulated CW counterpart, it will generate a higher signal-to-noise ratio. Also, time of flight measurement of such pulses can be used for coarse range measurements, and hence supports the triangulation algorithm. In other words, the quasi-CW approach combines

the advantages of PToF lidars and CW lidars without using and frequency, phase, or amplitude scanning and provides precise measurements at ranges far beyond the coherence length of the laser. Overall, when the long-range operation, high point cloud density requirements, and narrow time window conditions are considered the PB-MTCW technique is a potential candidate that can satisfy these requirements, whether it is a ground-based application or an airborne lidar system [40].

Funding. Office of Naval Research (N00014-18-1-2845).

Disclosures. The authors declare that there are no conflicts of interest related to this article.

Data Availability. Data underlying the results presented in this paper are not publicly available at this time but may be obtained from the authors upon reasonable request.

Supplemental document. See [Supplement 1](#) for supporting content.

References

1. C. Urmsom, J. Anhalt, D. Bagnell, C. Baker, R. Bittner, M. Clark, J. Dolan, D. Duggins, T. Galatali, and C. Geyer, "Autonomous driving in urban environments: Boss and the urban challenge," *J. Field Robotics* **25**(8), 425–466 (2008).
2. J. Hecht, "Lidar for self-driving cars," *Opt. Photonics News* **29**(1), 26–33 (2018).
3. L. Wallace, A. Lucieer, C. Watson, and D. Turner, "Development of a UAV-LiDAR system with application to forest inventory," *Remote Sens.* **4**(6), 1519–1543 (2012).
4. J. L. Bufton, J. B. Garvin, J. F. Cavanaugh, L. A. Ramos-Izquierdo, T. D. Clem, and W. B. Krabill, "Airborne lidar for profiling of surface topography," *Opt. Eng.* **30**(1), 72–79 (1991).
5. Y. Jiang, S. Karpf, and B. Jalali, "Time-stretch LiDAR as a spectrally scanned time-of-flight ranging camera," *Nat. Photonics* **14**(1), 14–18 (2020).
6. B. Behroozpour, P. A. Sandborn, M. C. Wu, and B. E. Boser, "Lidar system architectures and circuits," *IEEE Commun. Mag.* **55**(10), 135–142 (2017).
7. D. J. Lum, S. H. Knarr, and J. C. Howell, "Frequency-modulated continuous-wave LiDAR compressive depth-mapping," *Opt. Express* **26**(12), 15420–15435 (2018).
8. C. V. Poulton, A. Yaacobi, D. B. Cole, M. J. Byrd, M. Raval, D. Vermeulen, and M. R. Watts, "Coherent solid-state LIDAR with silicon photonic optical phased arrays," *Opt. Lett.* **42**(20), 4091–4094 (2017).
9. E. W. Mitchell, M. S. Hoehler, F. R. Giorgetta, T. Hayden, G. B. Rieker, N. R. Newbury, and E. Baumann, "Coherent laser ranging for precision imaging through flames," *Optica* **5**(8), 988–995 (2018).
10. K. Rainey, S. Gilbertson, D. Kalb, and T. Beery, "Modulation based ranging for direct displacement measurements of a dynamic surface," *Opt. Express* **29**(14), 21174–21189 (2021).
11. R. D. Peters, O. P. Lay, S. Dubovitsky, J. P. Burger, and M. Jeganathan, "MSTAR: an absolute metrology sensor with sub-micron accuracy for space-based applications," *Proc SPIE* **10568**, 105682O (2004).
12. J. Liu, Q. Sun, Z. Fan, and Y. Jia, "TOF Lidar development in autonomous vehicle," in *IEEE 3rd Optoelectronics Global Conference (OGC)* (2018) pp. 185–190.
13. M.-C. Amann, T. M. Bosch, M. Lescure, R. A. Myllylae, and M. Rioux, "Laser ranging: a critical review of unusual techniques for distance measurement," *Opt. Eng.* **40**, 10 (2001).
14. S. Kakuma, "Frequency-modulated continuous-wave laser radar using dual vertical-cavity surface-emitting laser diodes for real-time measurements of distance and radial velocity," *Opt. Rev.* **24**(1), 39–46 (2017).
15. D. H. Dolan, "Accuracy and precision in photonic Doppler velocimetry," *Rev. Sci. Instrum.* **81**(5), 053905 (2010).
16. Y.-S. Jang, J. Park, and J. Jin, "Sub-100-nm precision distance measurement by means of all-fiber photonic microwave mixing," *Opt. Express* **29**(8), 12229–12239 (2021).
17. J. P. Godbaz, M. J. Cree, and A. A. Dorrington, "Understanding and ameliorating non-linear phase and amplitude responses in amcw lidar," *Remote Sens.* **4**(1), 21–42 (2012).
18. A. Hymans and J. Lait, "Analysis of a frequency-modulated continuous-wave ranging system," *Proc. IEE, B Electron. Commun. Eng. UK* **107**(34), 365–372 (1960).
19. P. A. Roos, R. R. Reibel, T. Berg, B. Kaylor, Z. W. Barber, and W. R. Babbitt, "Ultrabroadband optical chirp linearization for precision metrology applications," *Opt. Lett.* **34**(23), 3692–3694 (2009).
20. P. Adany, C. Allen, and R. Hui, "Chirped lidar using simplified homodyne detection," *J. Lightwave Technol.* **27**(16), 3351–3357 (2009).
21. Z. W. Barber, W. R. Babbitt, B. Kaylor, R. R. Reibel, and P. A. Roos, "Accuracy of active chirp linearization for broadband frequency modulated continuous wave lidar," *Appl. Opt.* **49**(2), 213–219 (2010).
22. M. Harris, G. Pearson, J. Vaughan, D. Letalick, and C. Karlsson, "The role of laser coherence length in continuous-wave coherent laser radar," *J. Mod. Opt.* **45**(8), 1567–1581 (1998).
23. J. Riemensberger, A. Lukashchuk, M. Karpov, W. Weng, E. Lucas, J. Liu, and T. J. Kippenberg, "Massively parallel coherent laser ranging using a soliton microcomb," *Nature* **581**(7807), 164–170 (2020).
24. J. Armstrong, "Theory of interferometric analysis of laser phase noise," *J. Opt. Soc. Am.* **56**(8), 1024–1031 (1966).

25. T. Kim, P. Bhargava, and V. Stojanović, "Overcoming the Coherence Distance Barrier in Long-Range FMCW LIDAR," in (Optical Society of America, 2018), pp. STh3L-7.
26. E. Fischer, E. Dalhoff, and H. Tiziani, "Overcoming coherence length limitation in two wavelength interferometry—an experimental verification," *Opt. Commun.* **123**(4-6), 465–472 (1996).
27. X. Fan, Y. Koshikiya, and F. Ito, "Phase-noise-compensated optical frequency-domain reflectometry," *IEEE J. Quantum Electron.* **45**(6), 594–602 (2009).
28. M. Pu, W. Xie, L. Zhang, Y. Feng, Y. Meng, J. Yang, H. Zhou, Y. Bai, T. Wang, and S. Liu, "Dual-Heterodyne Mixing Based Phase Noise Cancellation for Long Distance Dual-Wavelength FMCW Lidar," in *Optical Fiber Communication Conference* (Optical Society of America, 2020), pp. Th1K-2.
29. J. T. Spollard, L. E. Roberts, C. S. Sambridge, K. McKenzie, and D. A. Shaddock, "Mitigation of phase noise and Doppler-induced frequency offsets in coherent random amplitude modulated continuous-wave LiDAR," *Opt. Express* **29**(6), 9060–9083 (2021).
30. R. Torun, M. M. Bayer, I. U. Zaman, J. E. Velazco, and O. Boyraz, "Realization of Multitone Continuous Wave Lidar," *IEEE Photonics J.* **11**(4), 1–10 (2019).
31. M. M. Bayer, R. Torun, X. Li, J. E. Velazco, and O. Boyraz, "Simultaneous ranging and velocimetry with multi-tone continuous wave lidar," *Opt. Express* **28**(12), 17241–17252 (2020).
32. M. M. Bayer and O. Boyraz, "Ranging and velocimetry measurements by phase-based MTCW lidar," *Opt. Express* **29**(9), 13552–13562 (2021).
33. M. M. Bayer, R. Torun, I. U. Zaman, and O. Boyraz, "A Basic Approach for Speed Profiling of Alternating Targets with Photonic Doppler Velocimetry," in *Conference on Lasers and Electro-Optics (CLEO)* (2019), p. AW4 K.4.
34. R. Torun, M. M. Bayer, I. U. Zaman, and O. Boyraz, "Multi-tone modulated continuous-wave lidar," *Proc. SPIE* **10925**, 109250V (2019).
35. O. Boyraz, M. M. Bayer, R. Torun, and I. Zaman, "TuD2.2 - Multi Tone Continuous Wave Lidar," in *IEEE Photonics Society Summer Topical Meeting Series (SUM)* (2019), pp. 1–2.
36. M. M. Bayer, R. Torun, I. U. Zaman, and O. Boyraz, "Multi-Tone Continuous Wave Lidar in Simultaneous Ranging and Velocimetry," in *Conference on Lasers and Electro-Optics (CLEO)* (2020), p. SM1O.6.
37. M. M. Bayer, G. N. Guentchev, X. Li, J. E. Velazco, and O. Boyraz, "Enhancing the multi-tone continuous-wave lidar with phase detection," *Proc. SPIE* **11828**, 1182807 (2021).
38. A. Dieckmann, "FMCW-LIDAR with tunable twin-guide laser diode," *Electron. Lett.* **30**(4), 308–309 (1994).
39. F. Gustafsson, "Determining the initial states in forward-backward filtering," *IEEE Trans. Signal Process.* **44**(4), 988–992 (1996).
40. G. Guentchev, M. M. Bayer, X. Li, and O. Boyraz, "Mechanical design and thermal analysis of a 12U CubeSat MTCW lidar based optical measurement system for littoral ocean dynamics," *Proc. SPIE* **11832**, 118320B (2021).